Journal of Colloid and Interface Science 580 (2020) 583–591

Contents lists available at ScienceDirect

Journal of Colloid and Interface Science

journal homepage: www.elsevier.com/locate/jcis

Photoelectrochemical immunosensor for sensitive detection of alpha-fetoprotein based on a graphene honeycomb film

Yilun Wu [a], He Su [a], Junfeng Yang [a], Zengyuan Wang [a], Daguang Li [a], Hang Sun [b], Xingyuan Guo [a], Shengyan Yin [a,*]

[a] State Key Laboratory on Integrated Optoelectronics, College of Electronic Science and Engineering, Jilin University, Changchun, Jilin 130012, China
[b] Key Laboratory of Bionic Engineering (Ministry of Education), College of Biological and Agricultural Engineering, Jilin University, Changchun, Jilin 130022, PR China

HIGHLIGHTS

- A photoelectrochemical electrode was fabricated based on a graphene honeycomb film.
- A fluorescent probe (AFP-PFBT-GOD) was synthesized for the detection current promotion.
- This photoelectrochemical biosensor can sensitively detect alpha-fetoprotein by competitive immunoassay.
- The photoelectrochemical biosensor has high detection sensitivity and good reliability.
- The detection limit of alpha-fetoprotein is lower than 0.05 ng/mL.

GRAPHICAL ABSTRACT

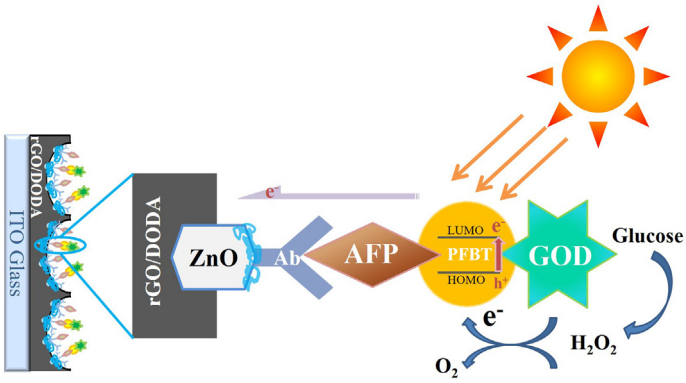

ARTICLE INFO

Article history:
Received 21 May 2020
Revised 12 July 2020
Accepted 13 July 2020
Available online 16 July 2020

Keywords:
Graphene
Honeycomb structure
Alpha-fetoprotein
Photoelectrochemical detection
Polymer nanoparticle

ABSTRACT

Alpha-fetoprotein (AFP) in adult serum often appears in early liver cancer. Therefore, early detection of an abnormal elevation of AFP concentration is important for the early diagnosis and treatment of primary liver cancer. In this work, a photoelectrochemical (PEC) electrode was fabricated for AFP-sensitive detection based on a reduced graphene oxide (rGO) honeycomb structure. After layer-by-layer bioconjugation, the immunoassay graphene electrode was modified with anti-AFP antibodies (Ab). Meanwhile, polymer nanoparticles (PFBT dots) were prepared *via* a nanoprecipitation method. In addition, the AFP was modified by using the PFBT dots and glucose oxidase (GOD), which formed a fluorescent probe (AFP-PFBT-GOD). By the competitive linkage of AFP and AFP-PFBT-GOD onto the anti-AFP modified honeycomb structure electrode, an immunosensor for AFP detection was obtained. During the PEC test, the electrons produced by the catalytic reaction of glucose and GOD can scavenge the photogenerated holes on the PFBT dots, which can reduce the recombination of photogenerated holes and electrons on the PFBT dots. The PEC immunosensor based on a rGO honeycomb structure exhibited a linear detection range of 0.05–100 ng/mL with a detection limit of 0.05 ng/mL. The excellent detection performance of the graphene PEC biosensor provides an opportunity for the early diagnosis of primary liver cancer.

1. Introduction

Alpha-fetoprotein (AFP) is an important biomarker for primary liver cancer [1]. AFP is mainly synthesized in the foetal liver and

* Corresponding author.
E-mail address: syyin@jlu.edu.cn (S. Yin).

https://doi.org/10.1016/j.jcis.2020.07.064
0021-9797/

yolk sac and then is normally found in foetal blood circulation, but it is almost non-existent in healthy adult serum [2]. Some studies reveal that the abnormal elevation of the AFP concentration in adult serum makes a significant association with cancer lesions, especially liver cancer. Since such an elevation often appears in early cancer, the early detection of an abnormal elevation of AFP concentration is important for early diagnosis and treatment of primary liver cancer [3,4]. However, this meaningful work is difficult to carry out by routine inspection methods due to the extremely low density of AFP. Therefore, many low concentration detection techniques have been developed to solve this situation, such as enzyme-linked immunoassay (ELISA), electrochemical luminescence (ECL), electrochemical method, and surface plasmon resonance (SPR) immunity determination [5–7]. These methods are confirmed to realize extra sensitive detection; nonetheless they are too complicated for instant analysis. Compared to these methods, photoelectrochemical (PEC) detection is a simple and efficient way to deal with the task of detecting the aforementioned AFP concentration, which has been widely used for the detection of biological molecules like glucose, ascorbic acid, cysteine, AFP and carcinoembryonic antigen [8,9]. Additionally, PEC detection relies on two processes, i.e., the photoelectric reaction and electrochemical reaction. The former requires a substrate with good light absorption and conversion ability, and the latter requires a more reactive material linkage. Furthermore, the introduction of a fluorescence probe can lead to an auxiliary enhancement of the detection current and promote the detection sensitivity.

Graphene is a widely used material that had remained undiscovered and hidden in natural graphite for a long time. In 2004, Geim and his assistants first discovered graphene through a micromechanical stripping method [10]. Although some properties of graphene have been revealed to be similar to graphite, graphene also shows many properties that are superior to graphite, such as extremely high boiling point, excellent thermal/electrical conductivity and good chemical stability [11]. These outstanding properties are attributed to the unique single-layer structure of graphene and the sp^2 hybridization of its in-layer carbon atoms [12]. In addition, graphene also shows a unique high specific surface area, extreme mechanical strength and good material compatibility [11,13,14]. Following its discovery, graphene has become one of the most promising carbon nanomaterials [2,15,16]. Actually, the planar structure and abundant edge defects in graphene results in a large number of heterogeneous material binding sites [17], which means that it is easily modified with semiconductors, metals and even biomolecules [18]. After being modified by functional materials, some graphene compound materials with excellent properties have been obtained [19–21]. Recently, Li designed label-free and sandwich-type electrochemical immunosensors based on a AuPt-vertical graphene/glassy carbon electrode for the quantification of AFP [22]. Moreover, Wang used a CdTe-loaded three-dimensional (3D) graphene hydrogel as a biosensor, which showed enhanced PEC performance [23]. These graphene-based materials are playing an increasingly more important role in energy storage, circuit control applications, photoelectric sensing, bioimaging, drug/gene transport therapy, stem cell engineering and other favourable fields [11,24–26].

In light of the abovementioned perception, we designed and fabricated a PEC electrode substrate based on a graphene honeycomb structure. Such a structure provides high surface area and improves light absorbance. In addition, this structure also reserves the extraordinary biocompatible and electrical properties of graphene and provides a stable pathway for electron transport. After a series procedure for biological modification, the graphene honeycomb structure electrode can be used to specifically identify AFP. On the other hand, a fluorescence probe (AFP-PFBT-GOD), namely polymer nanoparticles (PFBT dots) and glucose oxidase (GOD) modified onto AFP, was fabricated at the same time. Due to the competitive linkage of AFP and AFP-PFBT-GOD, an immunosensor for AFP detection was obtained. During the PEC test, when AFP-PFBT-GOD links onto the electrode, the PFBT dots can absorb visible light, resulting in the migration of many photogenerated electrons to the electrode, leaving behind photogenerated holes. Meanwhile, the electrons produced by the catalytic reaction of glucose and GOD can scavenge the photogenerated holes in the PFBT dots, which can reduce the recombination of photogenerated holes and electrons in the PFBT dots. Low AFP concentration detection was conducted via the competitive immune connection between AFP and AFP-PFBT-GOD to the substrate. The results show that the bio-inspired graphene electrode exhibits extremely high sensitivity and good reliability during the PEC detection.

2. Experimental section

2.1. Materials and characterization methods.

Hydrazine monohydrate ($N_2H_4{\cdot}H_2O$, 99%), glutaraldehyde (GLD, 50%), chitosan (CS), dimethyldioctadecylammonium (DODA, 97%), 1-ethyl-3-(3-dimethylaminopropyl) carbodiimide (EDC, 98%), and 4-(2-hydroxyethyl)-1-piperazineethanesulfonic acid (HEPES) were obtained from J&K Chemical Ltd. The high purity graphite (45 μm, 99.99%) was purchased from Thermo Fisher Scientific (Rockford, IL, U.S.A). Phosphate buffered saline (PBS) tablet, glucose oxidase (GOD), and bovine serum albumin (BSA) were purchased from Sigma-Aldrich. Potassium chloride (KCl), acetic acid (Ac), glucose, potassium peroxodisulfate ($K_2S_2O_8$), zinc nitrate ($Zn(NO_3)_2$), sodium hydroxide (NaOH), phosphorus pentoxide (P_2O_5), potassium permanganate ($KMnO_4$), potassium ferricyanide ($K_3[Fe(CN)_6]$), potassium ferrocyanide ($K_4[Fe(CN)_6]$), hydrochloric acid, sulfuric acid and all organic solvents were obtained from Beijing Chemical Works. Alpha-fetoprotein (AFP) and anti-AFP antibodies (Ab) were purchased from the Beijing Boisynthese Biotechnology Co., Ltd. Deionized water (resistance $\geq$ 18.25 MΩ cm^{-1}, PINGCHENG pure technology Co. LTD) was used for the whole experiment. ITO (indium tin oxide, resistance = 10 Ω) glasses were purchased from a local company. poly[(9,9-dioctylfluorenyl-2,7-diyl)-co-(1,4-benzo-[2,1′,3]-thiadazole)] (PFBT) and poly (styreneco-maleic anhydride) (PSMA) were bought from American Dye Source, Inc. (ADS).

Scanning electron microscope (SEM) images were obtained by using a JEOL JSM-7500F. Transmission electron microscopy (TEM) images for ZnO NCs and PFBT dots were taken by using a JEOL JEM-2100F. Optical imaging for the rGO/DODA honeycomb film was captured by an OLYMPUS BX51M metalloscope. The reflectance spectra and UV–visible light absorption were measured by a SHIMADZU UV-3600 and UNICO UV-4802, respectively, which covered a broad wavelength range of 200–800 nm. Fourier-transform infrared (FTIR) absorption spectra were evaluated by a SHIMADZU IR Affinity over the wavenumber range of 1000–4000 cm^{-1}.

2.2. Fabrication of the PEC electrode

The PEC electrode was fabricated through the breath figure method, followed by the use of a layer by layer method with biocompatible materials. First, 5 mg/mL graphene oxide aqueous solution was synthesized by two-step oxidation [27], and a 5 μg/mL ZnO nanocrystal (ZnO NCs; absorption spectrum and TEM image are exhibited in Fig. S1B) ethanol solution was synthesized by the Pacholski method[28], respectively. Then, a graphene oxide/dimethyldioctadecylammonium (GO/DODA) complex was prepared by a phase transfer method, which has been described in previous

articles [29]. The honeycomb structure was fabricated by the breath figure method [30]. Briefly, 20 μL GO/DODA chloroform solution (1 mg/mL) was drop cast onto ITO glass under wet airflow (relative humidity of approximately 85%). After all the solvent was volatilized, a brown film was left behind on the ITO glass. This film is the honeycomb structure with a highly ordered porous structure. These films were then reduced with hydrazine monohydrate at 90 °C. After 12 h of reaction, the tawny round items were transformed into black round items (Fig. 1A), indicating that the GO had turned into reduced graphene oxide (rGO). The surface morphology is shown in Fig. 1B and the Raman spectrum of the rGO/DODA honeycomb film is exhibited in Fig. 1C. Next, 0.2 mL ZnO NC ethanol solution was drop cast onto the honeycomb film, and then the film was annealed at 100 °C for 2 h. The 5 wt% chitosan (CS) acetic acid solution was used as a modifier agent to promote the biocompatibility of the abovementioned film. After drying in air, the honeycomb film was rinsed with diluted NaOH solution (0.01 mol/L) to fix the CS molecules. After activation by 5% glutaraldehyde aqueous solution, the anti-AFP antibodies (Ab) were linked onto the film, and, finally, the nonselective binding sites in the film were blocked with bovine serum albumin (BSA). The obtained graphene honeycomb film was used as an electrode for PEC detection. For comparison, a smooth rGO/DODA film was prepared under a dry environment (relative humidity lower than 30%). There were no pores on the smooth film (as shown in Fig. S2). After the same bioconjugation process, this smooth film was also used as a working electrode during PEC detection for control experiments.

2.3. Preparation of the AFP fluorescence probe (AFP-PFBT-GOD)

The polymer (poly[(9,9-dioctylfluorenyl-2,7-diyl)-co-(1,4-benzo-[2,1′,3]-thiadazole)], PFBT) nanoparticles (PFBT dots) were prepared *via* a nanoprecipitation method (Fig. S3) [31,32], and the diameter of the PFBT dots was adjusted to 26 nm (Fig. S4) with

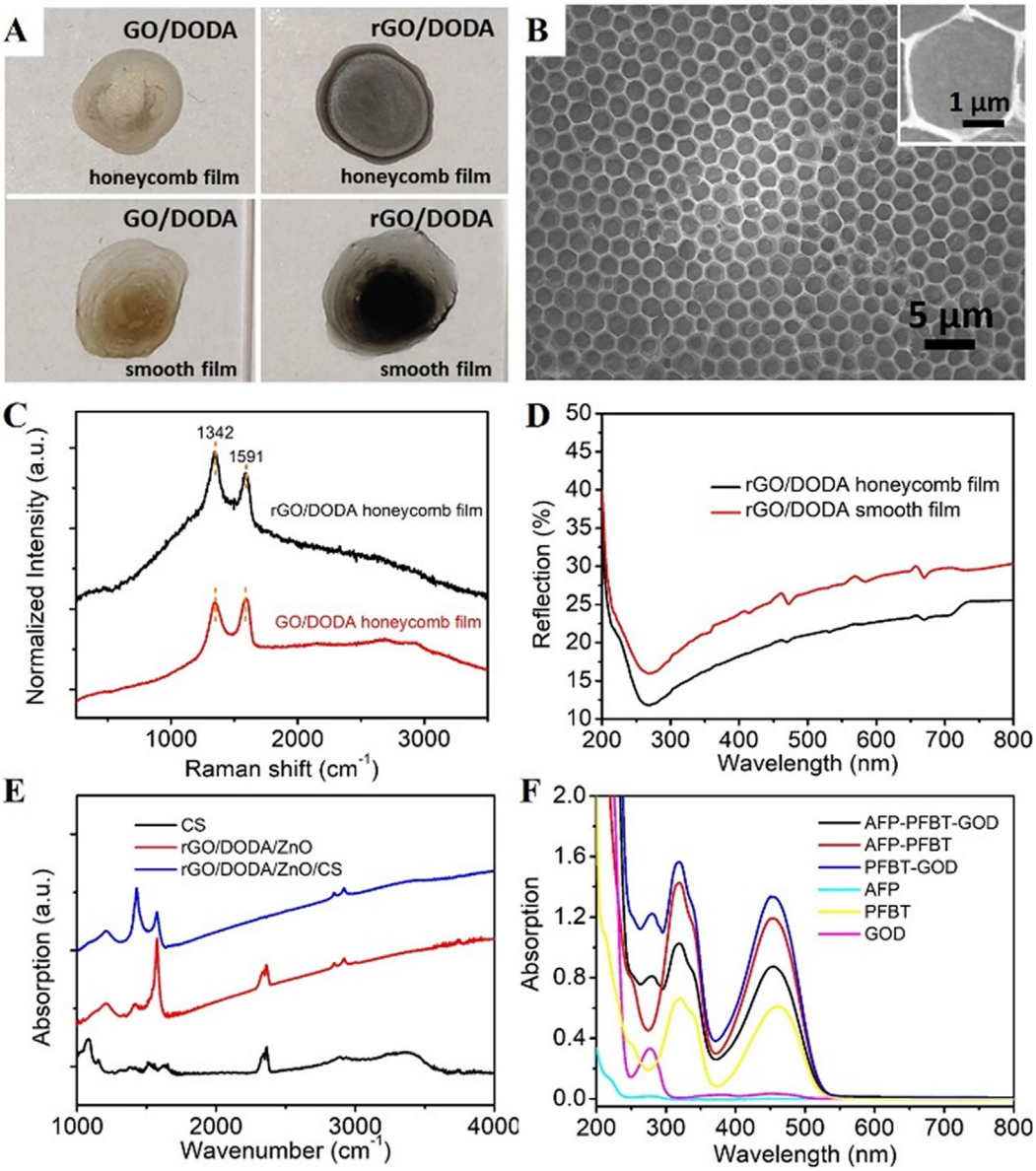

Fig. 1. (A) Optical photos of GO/DODA and rGO/DODA films; (B) SEM image of the rGO/DODA honeycomb film (inset shows the high-resolution SEM image of the honeycomb pore); (C) Raman spectra measured for the GO/DODA honeycomb film before and after reduction, respectively; (D) Reflection spectra for the rGO/DODA honeycomb film and smooth film; (E) FTIR spectra for the CS, rGO/DODA/ZnO and rGO/DODA/ZnO/CS; (F) UV–visible absorption spectra for the AFP, PFBT dots, GOD, AFP-PFBT, PFBT-GOD and AFP-PFBT-GOD composite.

the assistance of poly(styreneco-maleic anhydride) (PSMA) doping [33]. Many hydrophilic groups, such as carboxyl groups, were exposed outside of these PFBT dots. These carboxyl groups enabled easy dispersal of PFBT dots in water for the intermolecular repulsion, and, further, enabled easy connection with biomolecules. The concentration of the PFBT dot solution was measured from the absorption spectrum and was diluted to 50 ppm. Three different biomarkers, AFP-PFBT, PFBT-GOD, and AFP-PFBT-GOD were prepared using 1-ethyl-3-(3-dimethylaminopropyl) carbodiimide (EDC) as a catalyst to catalyse the linkage of biomacromolecules onto PFBT dots in a HEPES buffer solution (pH = 7.2), respectively. After dialysis for 48 h, most redundant small molecules were removed. The relative details for the preparation are provided in Supporting Information. The concentration of the obtained AFP-PFBT-GOD probe was adjusted to 1 ng/mL, and this concentration was used in all subsequent experiments.

2.4. Photocurrent measurements

All the PEC measurements were carried out by using a typical three-electrode system with the help of an electrochemical workstation (CHI 660E). A Pt electrode and Ag/AgCl electrode (3.0 M KCl) were used as counter and reference electrodes, respectively. The prepared PEC detection electrodes were used as working electrodes. Additionally, three kinds of electrolyte: KCl (0.1 M) solution containing a 5 mM $K_3[Fe(CN)_6]$-$K_4[Fe(CN)_6]$ (1:1) mixture, 0.1 M PBS (pH = 7.4) solution containing 60 mM glucose, and 0.1 M HCl solution containing 5 mM $K_3[Fe(CN)_6]$ were used for a series of electrochemical measurements. A high-pressure Xe lamp (300 W, CEAULIGHT, Co., Ltd.), which was equipped with a visible light filter ($\lambda > 420$ nm) was used as the excitation light source. The light intensity was approximately 100 mW/cm^2 in all experiments. The working electrodes were prepared via the following steps: a mixing solution containing the AFP solution (15 μL, a certain concentration) and AFP-PFBT-GOD (10 μL, 1 ng/mL) was drop cast onto the as-prepared electrode substrate and incubated for 30 min at 37 °C to obtain the photoelectrochemical detection electrode. Subsequently, the electrode was rinsed in 0.1 M PBS solution to remove unconnected AFP-PFBT-GOD composite. This electrode was then used as the working electrode. Photocurrent measurements were carried out using a 300 W Xe lamp to provide simulated solar irradiation and 0.1 M PBS solution containing 60 mM glucose as the electrolyte at a bias potential of 0.6 V at room temperature.

3. Results and discussion

3.1. Characterization of the rGO/DODA honeycomb film electrode and AFP-PFBT-GOD fluorescence probe.

The fabrication process for the graphene honeycomb film (rGO/DODA film) electrode and preparation for the AFP fluorescent probe label (AFP-PFBT-GOD) are shown in Scheme 1. During the fabrication process, each component of the biomolecules was applied onto the rGO/DODA honeycomb film electrode through the layer by layer method, which provided a strong and reliable conductive substrate with a regular anti-reflection structure. A thin good biocompatibility nanoparticle layer, ZnO NC layer, was inserted between the rGO/DODA honeycomb film layer and biomolecule for ensuring a better connection between the biomolecules and the graphene film. The AFP-PFBT-GOD fluorescence probes were prepared at the same time, which can connect with anti-AFP Ab in the same way as for pure AFP. The AFP-PFBT-GOD probe shows photoresponse and glucose sensitivity properties, which can enhance the PEC current. By mixing the sample solution with a certain concentration of AFP-PFBT-GOD followed by incubation in the electrode, these two types of AFP target competed for limited antibody combination sites. A higher AFP density can inhibit connection of the AFP-PFBT-GOD probes, which can induce a corresponding current change during PEC detection.

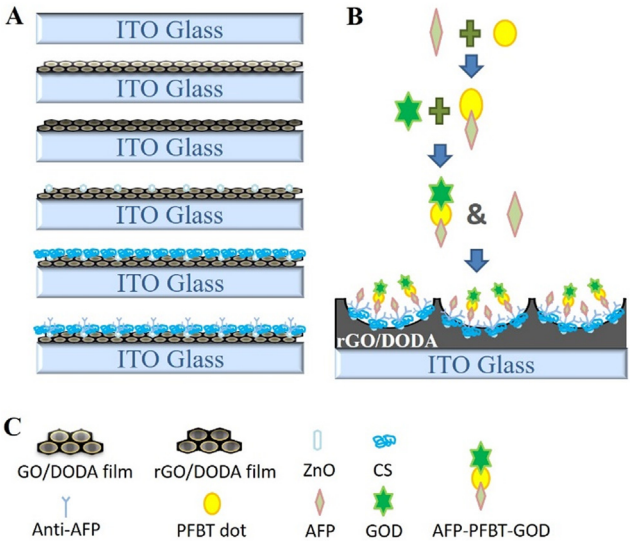

Scheme 1. (A) Fabrication of the PEC electrode; (B) Preparation of the AFP-PFBT-GOD fluorescent probe, and the competitive linkage of AFP and AFP-PFBT-GOD on the graphene honeycomb structure electrode; (C) Description of the illustration.

Optical images of the GO/DODA and rGO/DODA films are shown in Fig. 1A. All these films were formed on ITO glass, and significant differences can be found in these images. The GO/DODA films exhibited a totally brown colour, and, after chemical reduction, this colour changed to black, which is almost the colour of graphene. Meanwhile, the honeycomb films exhibited an evidently uniform material distribution, while the smooth film exhibited a thick to thin gradient. The honeycomb film possessed a bigger homogeneous centre area compared to the smooth film, which was due to the periodical structure realized by the template formed by the water drops during the chloroform evaporation process. For investigating the morphology of the rGO/DODA honeycomb film, a high-resolution SEM image was collected simultaneously. Fig. 1B shows that such a film exhibits a honeycomb-like structure. The whole image presents regular periodical mosaic hexagon cells. Each cell possesses a sharp hexagonal frame (shown in Fig. 1B inset), with a diameter of approximately 2 μm. The Raman spectra for the honeycomb film are shown in Fig. 1C. Two prominent peaks are observed in the spectra at 1342 cm^{-1} and 1591 cm^{-1}, corresponding to the G and D bands of carbon, respectively [27]. The intensity ratio of these two peaks was used to confirm the reduction of the graphene oxide – usually, a larger I_D/I_G ratio indicates that GO is converted to rGO. From the Raman spectra, the I_D/I_G ratio was determined to be 0.85 and 1.06 before and after reduction, respectively, indicating that the honeycomb film was reduced already. These walled cells endowed the honeycomb structure with a relative anti-reflection property, which exhibited 5% less reflection than that of the smooth film (Fig. 1D). The less reflectivity of the honeycomb film can offer more light scattering, which can promote the use of incident light during PEC detection (Scheme 2A). It is interesting that this periodically ordered honeycomb structure was able to change the path of the incident light. As shown in Fig. S1A, a clear diffraction ring was observed upon laser irradiation of such a structure.

During the fabrication process for the PEC electrode, the CS layer is an important bridge between the inorganic material and

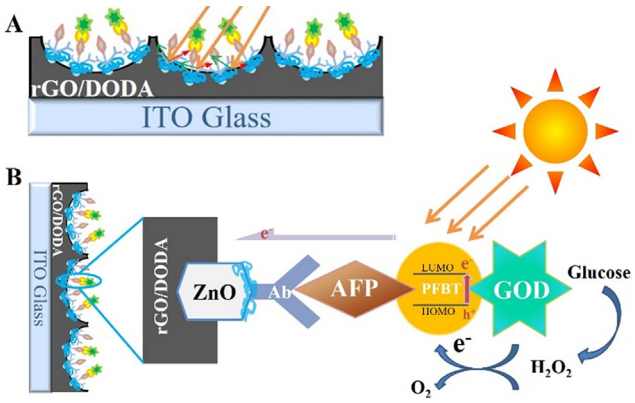

Scheme 2. (A) Mechanistic illustration of the incident light scattering; (B) Mechanism of PEC detection using an AFP-PFBT-GOD fluorescent probe.

organic biomolecules, whose bioactivity can be investigated by measurement of the FTIR absorption spectra. The FTIR data for CS, rGO/DODA/ZnO and rGO/DODA/ZnO/CS are shown in Fig. 1E. The absorption peak approximately 3360 cm^{-1} was attributed to the intermolecular hydrogen bonded –NH and –OH stretching vibration mode in the CS sample [34]. Meanwhile, amide I and amide II peaks located at 1627 cm^{-1} and 1518 cm^{-1} were found in the CS absorption, respectively. These two peaks are characteristic CS absorption peaks and were found to correspondingly exist in the rGO/DODA/ZnO/CS sample. This meant that CS had a good reserve of biological activity, which indicated the good biocapacity of the rGO/DODA/ZnO substrate [35]. Additionally, C—H stretching vibration peaks at 2880 cm^{-1} and 2930 cm^{-1} were also found to appear in the rGO/DODA/ZnO/CS and rGO/DODA/ZnO samples, which can be attributed to the long-chain alkanes of DODA in the honeycomb film [36].

The UV–visible absorption spectra for AFP, PFBT dots, GOD, AFP-PFBT, PFBT-GOD and AFP-PFBT-GOD composites were used to confirm the successful preparation of the AFP-PFBT-GOD composite. As shown in Fig. 1F, the absorption peaks for the PFBT dots are mainly located at 319 nm and 461 nm, which are regarded as the characteristic absorption peaks; these peaks were observed to remain exactly in the AFP-PFBT-GOD, AFP-PFBT, PFBT-GOD composites. Meanwhile, the AFP and GOD show absorption peaks at 220 nm and 280 nm, respectively, which are attributed to the protein characteristic absorption, i.e., the peptide bond and conjugated double bond absorption. These protein characteristic absorption peaks were, correspondingly, also observed in the three composites. The UV–visible spectra indicated a good connection amongst the AFP-PFBT-GOD fluorescence probe.

3.2. Characterizing the fabrication process for the photoelectrochemical biosensor

As shown in Scheme 2A, the incident light can be scattered by the honeycomb structure, and the scattered light will continuously stimulate the active ingredients, which are also stimulated by the incident light at the same time. The synergistic effects of the scattered light and incident light stimulation can enhance the light utilization. Similar effects have been reported in the literature [30]. In addition, the mechanism for the PEC detection process with the AFP-PFBT-GOD fluorescent probe is shown in Scheme 2B. The whole working electrode was immersed in a 60 mM glucose solution (resolved in 1 × PBS), which provided an abundant substrate for catalysed oxidation. With the catalysed oxidation of glucose, the mid-product H_2O_2 is generated rapidly. This instable oxyhydrogen is easily decomposed; meanwhile, many free electrons are released during the process of the catalysed oxidation of glucose. On the other hand, the electrons in the highest occupied molecule orbital (HOMO) of PFBT were excited into the lowest unoccupied molecular orbital (LUMO) with the exciting light irradiation. These electrons were then easily transported under the electric field. The lower reflectivity of the honeycomb film can offer more light scattering, which can promote the use of the incident light, thereby improving the number of photogenerated electrons. These extra free electrons can transfer into the existing graphene passageway, and, finally, be collected by the electrode, which can form an additional detection circuit with the impulse of bias voltage.

The fabrication process for the PEC biosensor electrodes was monitored by cyclic voltammetry. Cyclic voltammograms (CVs) measured for each step of the electrode fabrication are shown in Fig. S5A. The current response of the ITO glass is found to be the largest, which indicates that its resistance is far smaller than that of the subsequent functional layer, which will, thus, not influence the final electrode. This is the main reason why we used ITO as a basic substrate. After forming a GO/DODA honeycomb film on the ITO, the current response of the electrode is decreased rapidly, indicating that low conductivity of the GO material, which is consistent with theoretical values. The reduction step transformed the GO into rGO, which resulted in a rapid increase in the current density of the electrode. The ZnO NC modification process introduced a partial resistance and reduced the current density of the electrode. After the subsequent bio-modification process, the resulting current density was further reduced because of the low conductivity of the biomacromolecules. The observed change in the current density for all these electrodes suggested that the PEC electrode was successfully modified with the anti-AFP Ab. The corresponding electrochemical impedance spectroscopy (EIS) tests also confirmed the above results. As shown in Fig. S5B, all the data are represented by Nyquist plots. The curves consist roughly of two parts: an arc and a sloping line. The arc part is related to the measurement result under the high frequency condition, which reflects the charge transfer process of the electrode. A larger arc radius implies a slower charge transfer and a larger resistance for the electrode. As shown in the Nyquist plots, the arc radius in the electrode synthesis process exhibits a rapid increase (introduction of the GO/DODA honeycomb film) followed by a decrease (transition into rGO/DODA) and then gradual increase (introduction of biomacromolecules). The change in the charge transport resistance is consistent with the CV curve results.

The glucose enhancement response of the PEC electrode linked with a fluorescent probe in an abundant glucose environment is shown in Fig. 2A. An appropriate excitation light was applied to irradiate the working electrode. It can be seen that a current density of 50 $\mu A/cm^2$ was obtained in PBS solution. However, with the addition of 60 mM glucose, the current density was found to be significantly increased to approximately 100 $\mu A/cm^2$, which corresponds to a relative increase of 100%. This shows that the linkage of the glucose oxidase (GOD) part can meaningfully promote PEC detection.

The alteration of the photoelectric response of the PEC electrodes during the fabrication process provides the theoretical basis for subsequent biological detection. To clarify this clearly, the electrodes used for every step during the fabrication process were employed as the PEC electrode. The photoelectric response test outcomes for ITO, ITO/GO/DODA, ITO/rGO/DODA, ITO/rGO/DODA/ZnO, ITO/rGO/DODA/ZnO/CS, ITO/rGO/DODA/ZnO/CS/Ab, ITO/rGO/DODA/ZnO/CS/Ab/BSA ITO/rGO/DODA/ZnO/CS/Ab/BSA linked with AFP-PFBT, and ITO/rGO/DODA/ZnO/CS/Ab/BSA linked with AFP-PFBT-GOD are shown in Fig. 2B. It can be seen that the photoelectric response of ITO was merely 0.2 $\mu A/cm^2$, which did not affect subsequent electrodes. After the introduction of the GO/DODA honeycomb film, the photocurrent was increased to 0.4 $\mu A/cm^2$,

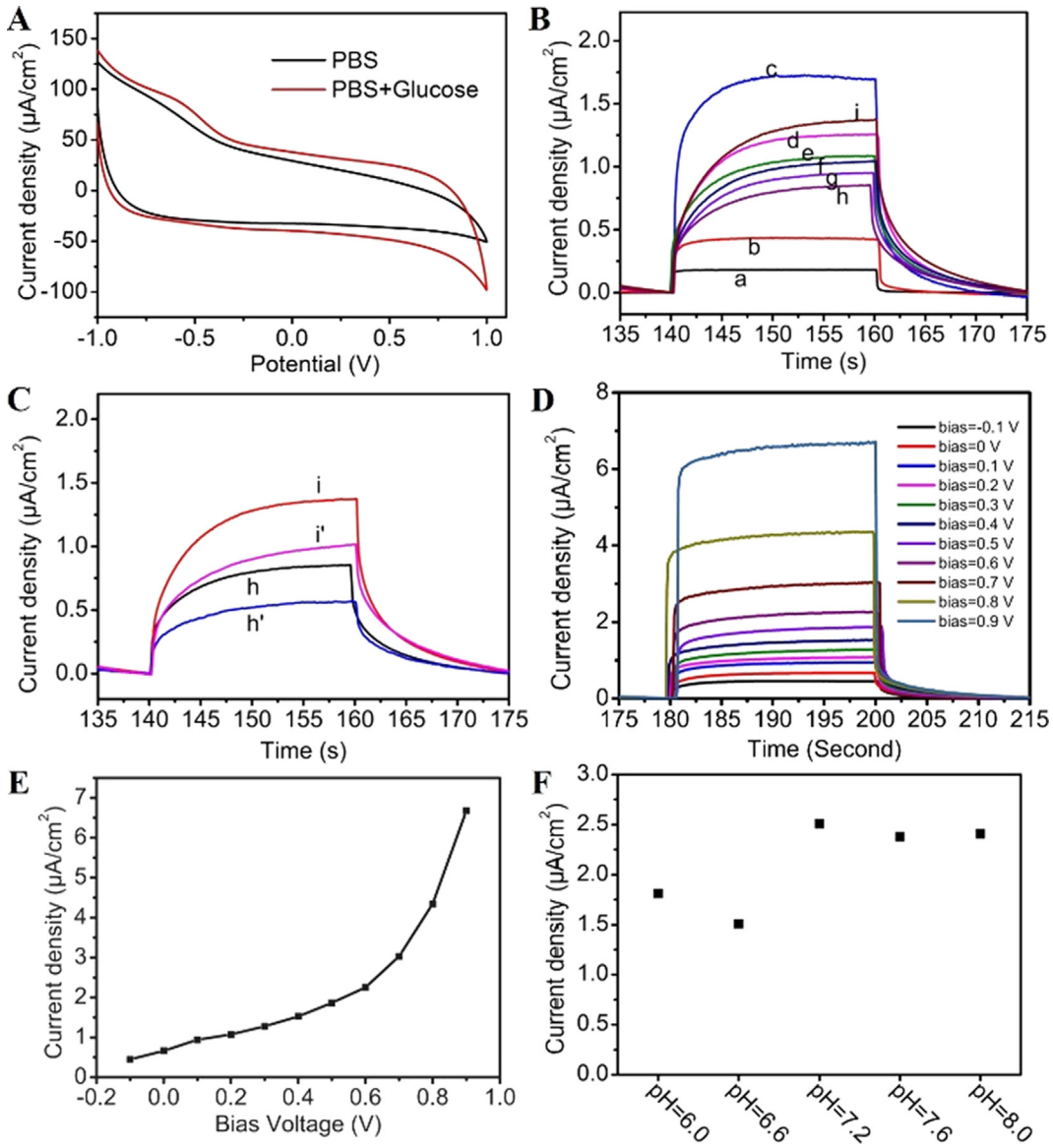

Fig. 2. (A) CV curves for the full detection substrate (ITO/rGO/DODA/ZnO/CS/Ab/BSA) linked with AFP-PFBT-GOD, measured in 0.1 M PBS with and without the presence of 60 mM glucose; (B) Photocurrent for the honeycomb film electrodes in 0.1 M PBS solution containing 60 mM glucose. The electrodes used in every test: (a) ITO, (b) ITO/GO/DODA, (c) ITO/rGO/DODA, (d) ITO/rGO/DODA/ZnO, (e) ITO/rGO/DODA/ZnO/CS (f) ITO/rGO/DODA/ZnO/CS/Ab, (g) ITO/rGO/DODA/ZnO/CS-/Ab/BSA, (h) ITO/rGO/DODA/ZnO/CS/Ab/BSA incubated with AFP-PFBT (10 μL, 1 ng/mL) and AFP (15 μL, 100 ng/mL) mixed solution, (i) ITO/rGO/DODA/ZnO/CS/Ab/BSA incubated with AFP-PFBT-GOD (10 μL, 1 ng/mL) and AFP (15 μL, 100 ng/mL) mixed solution; (C) Photocurrent measured for the honeycomb and smooth film electrodes in 0.1 M PBS solution containing 60 mM glucose. The electrodes used in every test: (h) ITO/rGO/DODA/ZnO/CS/Ab/BSA incubated with AFP-PFBT (10 μL, 1 ng/mL) and AFP (15 μL, 100 ng/mL) mixed solution, (i) ITO/rGO/DODA/ZnO/CS/Ab/BSA incubated with AFP-PFBT-GOD (10 μL, 1 ng/mL) and AFP (15 μL, 100 ng/mL) mixed solution, (h') ITO/smooth rGO/DODA/ZnO/CS/Ab/BSA incubated with AFP-PFBT (10 μL, 1 ng/mL) and AFP (15 μL, 100 ng/mL) mixed solution, and (i') ITO/smooth rGO/DODA/ZnO/CS/Ab/BSA incubated with AFP-PFBT-GOD (10 μL, 1 ng/mL) and AFP (15 μL, 100 ng/mL) mixed solution; (D) Photocurrent measured for honeycomb film electrodes at different potentials (−0.1 ~ 0.9 V) during the PEC measurements); (E) The curve for the maximum response photocurrent versus voltage; and (F) The photocurrent response for AFP detection (100 ng/mL) in 0.1 M PBS electrolyte with 60 mM glucose at different pH values.

and, successively, further increased to 1.75 μA/cm^2 after reduction to rGO/DODA, which was attributed to the high photon absorption of the honeycomb structure and conductivity of the graphene material. In fact, the in-layer conductivity of graphene can reach as high as 5×10^5 S/m [26], which provides good electron collection properties for the photoresponse process. After modification with ZnO, CS, Ab and BSA, the photocurrent was observed to be gradually reduced, until reaching a minimum value of 0.6 μA/cm^2 after connection with the AFP-PFBT probe, indicating that the presence of biomaterials led to a certainly obstruction effect for the charge transfer of the electrode. Furthermore, the rise in the photocurrent to the biggest response becomes slower for each electrode, indicating that the kinetics for the photoelectric response are decreased too. It is noticed that the electrode photocurrent increased back to 1.3 μA/cm^2 after linking with the AFP-PFBT-GOD probe, showing that the introduction of GOD had a significant improvement on the photoelectric response of the electrode. Moreover, the introduction of GOD also enhances the rate of the photoelectric response. The photocurrent enhancement effect is also the theoretical basis for our subsequent photoelectrochemical detection experiments. To investigate the role of the honeycomb structure, the honeycomb film and smooth film electrodes were applied for photoelectric response tests. As shown in Fig. 2C, the photocurrent of the honeycomb film electrodes is larger than

that of the smooth film electrodes, no matter of the electrodes are incubated in the AFP-PFBT and AFP mixed solution or in the AFP-PFBT-GOD and AFP mixed solution. These data indicated that the honeycomb structure had an obvious promotion effect during the photoelectrochemical detection due to the enhanced light utilization efficiency.

Normally, PEC tests are influenced by the experimental conditions; so, the experimental conditions need to be optimized. The effect of the applied bias voltage during the test is shown in Fig. 2D. Generally, the detection of photocurrent density increased with increasing bias voltage. Furthermore, sharp photocurrent response curves were observed during the alternating switch-on and switch-off events, which implied a rapid response. In addition, the maximum photocurrent density values at different biases with the light stimulation were smooth. The current density for the bias curve is shown in Fig. 2E. In the low-voltage region (−0.1 V ~ 0.6 V), such an increase was slight and exhibited a linear relationship with bias voltage. While the photocurrent response was found to rapidly increase at higher bias voltage (>0.6 V), with every 0.1 V of bias voltage increase leading to a 50% increase in detection current density. However, the remarkable increase in photocurrent was limited by the surface chemical procedure, i.e., H_2O oxidization. When the bias voltage was raised to above 0.9 V, many small bubbles were observed to be generated on the surface of the electrode, which can break the film structure and inactivate the biomolecule. For maintaining the duration of these film electrodes, and, in the meantime, ensuring the detection sensitivity, an appropriate bias voltage of 0.6 V was chosen.

The effect of the pH value of the detection environment was also explored. As shown in Fig. 2F, the photocurrent density was influenced by the solution pH value. A mild acidic or alkaline environment was found to inhibit the detection current, and the acidic solution seemingly led to an even greater influence on the electrode. From the results obtained for the control experiments with different pH values, the best detecting condition was ensured at pH = 7.2, which is also correspondent with a body fluid environment. Such a test result revealed that the PEC electrode is highly compatible with an in vivo environment. Meanwhile, this pH value was employed for the following AFP detection.

3.3. Photoelectrochemical detection of AFP

Considering the low target concentration, seven AFP concentration gradients (0.05 ng/mL, 0.1 ng/mL, 0.5 ng/mL, 1 ng/mL, 10 ng/mL, 50 ng/mL, and 100 ng/mL) were selected to evaluate the PEC detection performance. Specifically, the AFP-PFBT-GOD fluorescence probe was calibrated to an actual concentration containing 1 ng/mL AFP with the help of absorption spectra. Then, 15 μL of AFP solutions of various concentrations were taken and mixed with 10 μL of the above probe solution. This mixed solution was then drop cast onto an electrode and incubated for 30 min. After competitive immune linkage, the photocurrent density for these immunosensors was measured by a three-electrode system with an electrochemical workstation (CHI 660E). The PEC immunobiosensor electrode exhibited a higher photocurrent density after connection with the AFP-PFBT-GOD fluorescent probe compared to connection with AFP, which indicates good potential for competitive immunosensing. As shown in Fig. 3A, for an AFP concentration of 0.05 ng/mL, the photocurrent density was detected to be nearly 1.7 $\mu A/cm^2$. With increasing AFP concentration, the measured photocurrent density was found to decrease gradually, even falling to 0.83 $\mu A/cm^2$ when the concentration of AFP reached up to

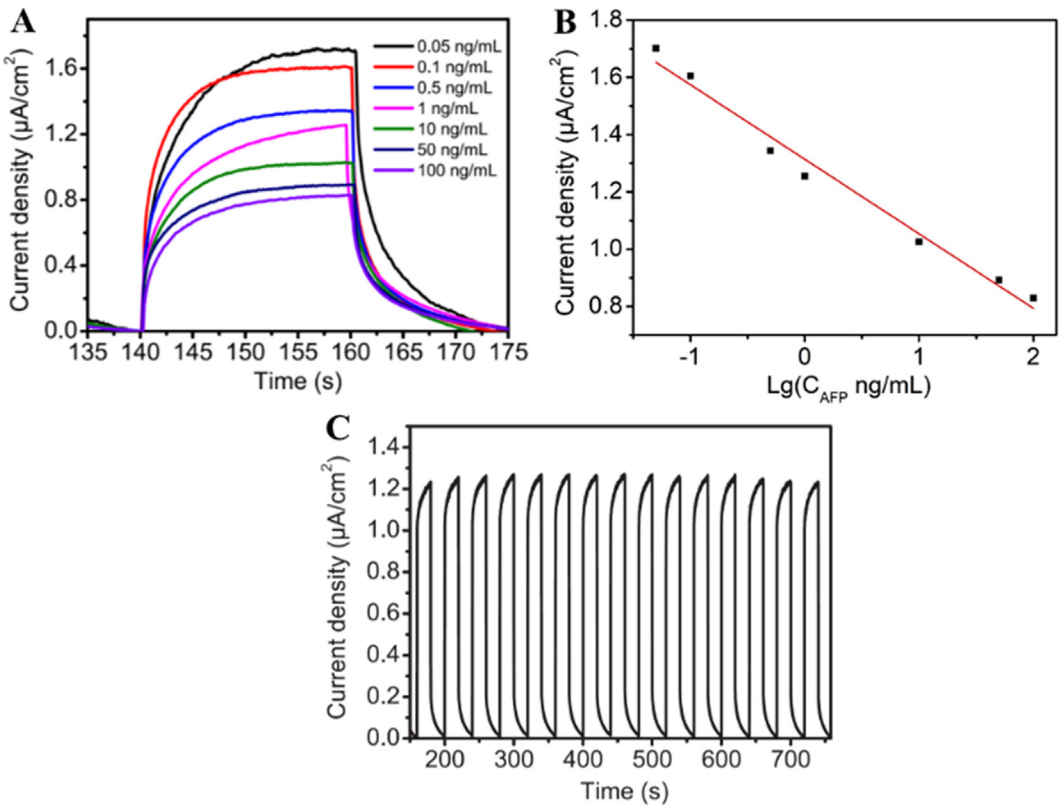

Fig. 3. (A) Photoelectric response curves obtained for different AFP concentrations; (B) Lg (C_{AFP} ng/mL) versus photocurrent density scatter-dot plots and corresponding linear fitting result (red line); and (C) cycle stability of the electrode for the detection of 100 ng/mL AFP. (For interpretation of the references to colour in this figure legend, the reader is referred to the web version of this article.)

100 ng/mL. By intercepting the maximum of the photocurrent density at each detection concentration and plotting it versus the logarithm of the AFP concentration, a scatter-dot diagram (Fig. 3B) was obtained, which showed a nearly straight-line distribution. Through the linear fitting, a corresponding linear equation for $\Delta I = 1.314–0.26 \lg (C_{AFP}$ ng/mL) was found. The fitting slope showed a standard deviation of 0.015. These PEC bioimmunosensors show good linear detection capacity, which can be used for precise AFP concentration measurements.

A parallel contrast was made among the 4 bioimmunosensor electrodes prepared by the same craft with a detection target of 100 ng/mL AFP. As shown in Fig. S6, the difference between all the test results is small, and its variance is lower than 0.1. To test the detection stability of the obtained PEC bioimmunosensor, a multi-cycle photocurrent detection test was carried out at the same time at a detection concentration of 100 ng/mL (Fig. 3C). As shown by the I-t curve, the electrode showed a highly consistent detection current density over a total of 15 cycles, maintaining a current value of approximately 1.23 $\mu A/cm^2$. These controlled experimental data indicate that the AFP bioimmunosensor possessed good stability, which is beneficial for measurements in clinical tests.

4. Conclusions

Previous studies have reported inverse opal electrodes with signal amplification provided by CdS-QDs [3] or $CsPbCl_3$ perovskite quantum dots [37] applied as photoelectrochemical electrodes, which show good AFP detection performance. In addition, a CdTe-loaded graphene hydrogel used as a biosensor has been shown to exhibit good PEC performance for miRNA detection [23], and a g-CN/rGO composite material has also been used to realize a dual mode competitive immunosensing platform for the determination of AFP [38]. However, there have been no reports for a PEC biosensor based on a graphene electrode with a hierarchical structure for AFP detection, and there are currently no reports for the use of metal-free probes in PEC testing. In our work, a PEC bioimmunosensor based on a graphene honeycomb structure film was designed and constructed. With the assistance of a surfactant, a graphene honeycomb structure film was constructed on ITO glass by the breath figure method. The graphene honeycomb structure shows good anti-reflection performance, which can make full use of incident light. Furthermore, the graphene honeycomb structure offers a better conductive substrate compared to that of the inverse opal electrodes. At the same time, AFP was modified with polymer nanoparticles (PFBT) and glucose oxidase (GOD) to prepare a fluorescence probe (AFP-PFBT-GOD), which can be used to enhance the photoelectric characteristics. This probe avoids the introduction of metal ions, which is beneficial to the biocompatibility. By using the competitive immunity method, the graphene honeycomb PEC bioimmunosensor was found to show good detection capacity for AFP in the concentration range of 0.05 ng/m L ~ 100 ng/mL and an AFP detection limit of lower than 0.05 ng/mL, which is comparable to that found for PEC electrodes composed of inverse opal electrodes and rGO composite materials [37,38]. This immunosensor based on a graphene bio-inspired film may be beneficial towards measurements in clinical tests or biological analysis research.

Declaration of Competing Interest

The authors declare that they have no known competing financial interests or personal relationships that could have appeared to influence the work reported in this paper.

Acknowledgment

This work was supported by the grants from the National Natural Science Foundation of China (Grant No. 51772121), and Jilin Provincial Science & Technology Department (20200401126GX).

Author contributions

Yilun Wu and He Su designed and performed the experiments, analyzed and interpreted the data, wrote the paper; Zengyuan Wang synthesized the fluorescence probe; Junfeng Yang performed the XRD measurements; Daguang Li performed the TEM measurements; Xingyuan Guo provided the analysis and interpretation of the EIS data; Hang Sun assisted with the analyses and together with Shengyan Yin supervised the work. All authors discussed the results and contributed to the scientific interpretation as well as to the writing of the manuscript. All authors reviewed the manuscript.

Appendix A. Supplementary data

Supplementary data to this article can be found online at https://doi.org/10.1016/j.jcis.2020.07.064.

References

[1] X.P. Liu, H.W. Wu, Y. Zheng, Z.S. Wu, J.H. Jiang, G.L. Shen, R.Q. Yu, A sensitive electrochemical immunosensor for alpha-fetoprotein detection with colloidal gold-based dentritical enzyme complex amplification, Electroanalysis 22 (2010) 244–250.
[2] C.B. Jacobs, M.J. Peairs, B.J. Venton, Review: Carbon nanotube based electrochemical sensors for biomolecules, Anal. Chim. Acta 662 (2010) 105–127.
[3] R. Xu, Y.D. Jiang, L. Xia, T.X. Zhang, L. Xu, S. Zhang, D.L. Liu, H.W. Song, A sensitive photoelectrochemical biosensor for AFP detection based on ZnO inverse opal electrodes with signal amplification of CdS-QDs, Biosens. Bioelectron. 74 (2015) 411–417.
[4] Z.Y. Guo, T.T. Hao, J. Duan, S. Wang, D.Y. Wei, Electrochemiluminescence immunosensor based on graphene-CdS quantum dots-agarose composite for the ultrasensitive detection of alpha fetoprotein, Talanta 89 (2012) 27–32.
[5] Z. Han, M. Luo, L. Chen, J. Chen, C. Li, A photoelectrochemical immunosensor for detection of α-fetoprotein based on Au-ZnO flower-rod heterostructures, Appl. Surf. Sci. 402 (2017) 429–435.
[6] H. Sha, Y. Wang, Y. Zhang, H. Ke, X. Xiong, N. Jia, Enzyme-free ECL immunesensor based on PbS nanocrystals for highly sensitive detection of alpha fetoprotein, Sensors Actuators B Chem. 277 (2018) 157–163.
[7] Y. Zhu, Q. Zhang, X. Li, H. Pan, J. Wang, Z. Zhao, Detection of AFP with an ultrasensitive giant magnetoimpedance biosensor, Sensors Actuators B Chem. 293 (2019) 53–58.
[8] J. Chen, G.-C. Zhao, A novel signal-on photoelectrochemical immunosensor for detection of alpha-fetoprotein by in situ releasing electron donor, Biosens. Bioelectron. 98 (2017) 155–160.
[9] J. Shu, D. Tang, Recent advances in photoelectrochemical sensing: from engineered photoactive materials to sensing devices and detection modes, Anal. Chem. 92 (2020) 363–377.
[10] K.S. Novoselov, A.K. Geim, S.V. Morozov, D. Jiang, Y. Zhang, S.V. Dubonos, I.V. Grigorieva, A.A. Firsov, Electric field effect in atomically thin carbon films, Science 306 (2004) 666–669.
[11] K.S. Novoselov, V.I. Fal'ko, L. Colombo, P.R. Gellert, M.G. Schwab, K. Kim, A roadmap for graphene, Nature 490 (2012) 192–200.
[12] K.S. Kim, Y. Zhao, H. Jang, S.Y. Lee, J.M. Kim, K.S. Kim, J.H. Ahn, P. Kim, J.Y. Choi, B.H. Hong, Large-scale pattern growth of graphene films for stretchable transparent electrodes, Nature 457 (2009) 706–710.
[13] J.H. Chen, C. Jang, S.D. Xiao, M. Ishigami, M.S. Fuhrer, Intrinsic and extrinsic performance limits of graphene devices on SiO2, Nat. Nanotechnol. 3 (2008) 206–209.
[14] G.X. Wang, B. Wang, J. Park, Y. Wang, B. Sun, J. Yao, Highly efficient and large-scale synthesis of graphene by electrolytic exfoliation, Carbon 47 (2009) 3242–3246.
[15] S.Y. Yin, Y.Y. Zhang, J.H. Kong, C.J. Zou, C.M. Li, X.H. Lu, J. Ma, F.Y.C. Boey, X.D. Chen, Assembly of Graphene Sheets into Hierarchical Structures for High-Performance Energy Storage, ACS Nano 5 (2011) 3831–3838.
[16] M. Orecchioni, C. Menard-Moyon, L.G. Delogu, A. Bianco, Graphene and the immune system: challenges and potentiality, Adv. Drug Delivery Rev. 105 (2016) 163–175.
[17] M. Buzaglo, I.P. Bar, M. Varenik, L. Shunak, S. Pevzner, O. Regev, Graphite-to-graphene: total conversion, Adv. Mater. 29 (2017) 1603528.

[18] L.L. Liu, Z.Q. Niu, L. Zhang, X.D. Chen, Structural diversity of bulky graphene materials, Small 10 (2014) 2200–2214.
[19] X.J. Men, Y.L. Wu, H.B. Chen, X.F. Fang, H. Sun, S.Y. Yin, W.P. Qin, Facile fabrication of TiO2/Graphene composite foams with enhanced photocatalytic properties, J. Alloy. Compd. 703 (2017) 251–257.
[20] M.G. Wang, J. Han, H.X. Xiong, R. Guo, Yolk@shell nanoarchitecture of Au@r-GO/TiO2 hybrids as powerful visible light photocatalysts, Langmuir 31 (2015) 6220–6228.
[21] H. Hu, Z.B. Zhao, W.B. Wan, Y. Gogotsi, J.S. Qiu, Ultralight and highly compressible graphene aerogels, Adv. Mater. 25 (2013) 2219–2223.
[22] D. Sun, H. Li, M. Li, C. Li, L. Qian, B. Yang, Electrochemical immunosensors with AuPt-vertical graphene/glassy carbon electrode for alpha-fetoprotein detection based on label-free and sandwich-type strategies, Biosens. Bioelectron. 132 (2019) 68–75.
[23] N. Hao, J. Lu, M. Chi, M. Xiong, Y. Zhang, R. Hua, K. Wang, A universal photoelectrochemical biosensor for dual microRNA detection based on two CdTe nanocomposites, J. Mater. Chem. B 7 (2019) 1133–1141.
[24] S.Z. Butler, S.M. Hollen, L.Y. Cao, Y. Cui, J.A. Gupta, H.R. Gutierrez, T.F. Heinz, S.S. Hong, J.X. Huang, A.F. Ismach, E. Johnston-Halperin, M. Kuno, V.V. Plashnitsa, R.D. Robinson, R.S. Ruoff, S. Salahuddin, J. Shan, L. Shi, M.G. Spencer, M. Terrones, W. Windl, J.E. Goldberger, Progress, challenges, and opportunities in two-dimensional materials beyond graphene, ACS Nano 7 (2013) 2898–2926.
[25] S.Y. Yin, Y.L. Wu, B.H. Hu, Y. Wang, P.Q. Cai, C.K. Tan, D.P. Qi, L.Y. Zheng, W.R. Leow, N.S. Tan, S.T. Wang, X.D. Chen, Three-dimensional graphene composite macroscopic structures for capture of cancer cells, Adv. Mate. Interfaces 1 (2014) 1300043.
[26] C. Cheng, S. Li, A. Thomas, N.A. Kotov, R. Haag, Functional graphene nanomaterials based architectures: biointeractions, fabrications, and emerging biological applications, Chem. Rev. 117 (2017) 1826–1914.
[27] X.J. Men, H.B. Chen, K.W. Chang, X.F. Fang, C.F. Wu, W.P. Qin, S.Y. Yin, Three-dimensional free-standing ZnO/graphene composite foam for photocurrent generation and photocatalytic activity, Appl. Catal. B-Environ. 187 (2016) 367–374.
[28] B. Nikoobakht, M.A. El-Sayed, Preparation and growth mechanism of gold nanorods (NRs) using seed-mediated growth method, Chem. Mater. 15 (2003) 1957–1962.
[29] S.Y. Yin, Z.Q. Niu, X.D. Chen, Assembly of graphene sheets into 3D macroscopic structures, Small 8 (2012) 2458–2463.
[30] S.Y. Yin, X.J. Men, H. Sun, P. She, W. Zhang, C.F. Wu, W.P. Qin, X.D. Chen, Enhanced photocurrent generation of bio-inspired graphene/ZnO composite films, J. Mater. Chem. A 3 (2015) 12016–12022.
[31] K. Landfester, R. Montenegro, U. Scherf, R. Guntner, U. Asawapirom, S. Patil, D. Neher, T. Kietzke, Semiconducting polymer nanospheres in aqueous dispersion prepared by a miniemulsion process, Adv. Mater. 14 (2002) 651–655.
[32] T. Kietzke, D. Neher, K. Landfester, R. Montenegro, R. Guntner, U. Scherf, Novel approaches to polymer blends based on polymer nanoparticles, Nat. Mater. 2 (2003) 408–U407.
[33] X.J. Zhang, J.B. Yu, C.F. Wu, Y.H. Jin, Y. Rang, F.M. Ye, D.T. Chiu, Importance of having low-density functional groups for generating high-performance semiconducting polymer dots, ACS Nano 6 (2012) 5429–5439.
[34] N. Benbettaieb, C. Tanner, P. Cayot, T. Karbowiak, F. Debeaufort, Impact of functional properties and release kinetics on antioxidant activity of biopolymer active films and coatings, Food Chem. 242 (2018) 369–377.
[35] C.D. Qiao, X.G. Ma, J.L. Zhang, J.S. Yao, Molecular interactions in gelatin/chitosan composite films, Food Chem. 235 (2017) 45–50.
[36] T.R. Zhang, W. Feng, Y.Q. Fu, R. Lu, C.Y. Bao, X.T. Zhang, B. Zhao, C.Q. Sun, T.J. Li, Y.Y. Zhao, J.N. Yao, Self-assembled organic-inorganic composite superlattice thin films incorporating photo- and electro-chemically active phosphomolybdate anion, J. Mater. Chem. 12 (2002) 1453–1458.
[37] J. Qin, S. Cui, X. Yang, G. Yang, Y. Zhu, Y. Wang, D. Qiu, CsPbCl3 perovskite quantum dots/TiO2 inverse opal photonic crystals for efficient photoelectrochemical detection of alpha fetoprotein, J. Phy. D: Appl. Phys. 52 (2019) 415101.
[38] H. Yan, L. Gong, L. Zang, H. Dai, G. Xu, S. Zhang, Y. Lin, Dual-responsive competitive immunosensor for sensitive detection of tumor marker on g-CN/rGO conjugation, Sensors Actuators B Chem. 230 (2016) 810–817.